

Residual foreground contamination in the WMAP data and bias in non-Gaussianity estimation

Pravabati Chingangbam^{1,2}

E-mail: prava@iiap.res.in

Changbom Park²

E-mail: cbp@kias.re.kr

¹ Indian Institute of Astrophysics, Koramangala II Block, Bangalore 560 034, India and

²Korea Institute for Advanced Studies, 85 Hoegiro, Dongdaemun-gu, Seoul 130-722, Korea

Abstract. We analyze whether there is any residual foreground contamination in the cleaned WMAP 7 years data for the differential assemblies, Q, V and W. We calculate the correlation between the foreground map, from which long wavelength correlations have been subtracted, and the foreground reduced map for each differential assembly after applying the Galaxy and point sources masks. We find positive correlations for *all* the differential assemblies, with high statistical significance. For Q and V, we find that a large fraction of the contamination comes from pixels where the foreground maps have positive values larger than three times the rms values. These findings imply the presence of residual contamination from Galactic emissions and unresolved point sources. We redo the analysis after masking the extended point sources catalogue of Scodeller *et al.* [7] and find a drop in the correlation and corresponding significance values. To quantify the effect of the residual contamination on the search for primordial non-Gaussianity in the CMB we add estimated contaminant fraction to simulated Gaussian CMB maps and calculate the characteristic non-Gaussian deviation shapes of Minkowski Functionals that arise due to the contamination. We find remarkable agreement of these deviation shapes with those measured from WMAP data, which imply that a major fraction of the observed non-Gaussian deviation comes from residual foreground contamination. We also compute non-Gaussian deviations of Minkowski Functionals after applying the point sources mask of Scodeller *et al* and find a decrease in the overall amplitudes of the deviations which is consistent with a decrease in the level of contamination.

1. Introduction

The cosmic microwave background (CMB) radiation and the large scale structures in the universe carry a wealth of cosmological information. Observational data support the cosmological models dominated by cold dark matter and the cosmological constant [1, 2] (see also [3] for a critical review of the current cosmological models). In the case of the CMB the correct extraction of cosmological information crucially depends on our ability to measure the true CMB signal. In practice, the experimentally observed CMB temperature fluctuations is composed of the true CMB signal and foreground signals coming from astrophysical sources that emit photons in the frequency ranges spanned by the observations. The major part of the foreground component comes from diffuse emissions from our Galaxy, and a small fraction comes from extra-Galactic point sources [4] such as radio galaxies and dusty star-forming galaxies. The Galaxy emissions consist of thermal and spinning dust emissions, free-free emissions from electrons-ion scattering, synchrotron radiation from shock accelerated electrons interacting with the Galactic magnetic field and a component called the ‘haze’ whose physical origin is not yet understood. These foreground components are usually estimated based on templates and then subtracted from the observed data [5].

The WMAP data release [6] includes masks for our Galaxy and for extra-Galactic point sources which have been identified [5]. Henceforth, we refer to the point sources mask provided by the WMAP team as PS1. Recently, Scodeller *et al.* [7] reported the detection of new point sources in the WMAP data that have not been reported before. They provide two extended masks [8], which we refer to as PS2 and PS3, and they include the sources identified by the WMAP team as subsets. PS2 has 1116 sources outside the KQ85 Galactic mask, which were detected either at 5σ directly in any of the 5 WMAP channels or at 5σ in internal templates and at 3σ in any of the channels. PS3 has 2102 sources outside the KQ85 Galactic mask, which were detected either at 5σ directly in any of the 5 WMAP channels or at 5σ in internal templates.

The goal of this paper is twofold. The first goal is to investigate whether there is small but statistically significant residual foreground contamination in the cleaned and masked WMAP data. Our method is based on calculating correlations between the foreground field, which has been processed so as to remove long wavelength correlations of the galaxy emissions, and the cleaned CMB data. Our basic premise is that if there is no residual contamination in the cleaned and masked data we should obtain no correlation. However, we find statistically significant positive correlation for WMAP 7 years data for the Q, V and W differential assemblies (DAs) where we have applied the KQ75 galactic mask and PS1. We further find that a big fraction (as big as 30% for Q channel) comes from regions where the foreground map has large positive values, which indicates unresolved point sources. These results give a clear indication that there are residual foreground contamination in the cleaned data. A brief report of these results has been presented in [9]. We redo the above calculation of correlation after applying PS2 and PS3. As is reasonable to expect, we find a decrease in the value of the

correlations and a corresponding decrease in the statistical significance of those values, implying that these newly identified point sources have non-trivial contribution to the correlations.

Our second goal is to study the effect of the residual contamination on the estimation of non-Gaussianity parameters by using Minkowski Functionals (MFs) [10, 11, 12, 13]. To this end we add estimated contaminant fraction to Gaussian CMB simulations and calculate their effect on the MFs. A comparison between the characteristic non-Gaussian deviation shapes of the MFS that result from the residual contamination and the non-Gaussian deviation shapes of WMAP data using PS1 reveals a remarkable similarity. From this we conclude that the non-Gaussian deviations seen in MFS measured from WMAP data must come predominantly from the residual foreground contamination. Further, in order to isolate the effect of the new point sources contained in PS2 and PS3 we redo the calculation of non-Gaussian deviation of MFs from WMAP data after masking them. We find that the first MF is very strongly affected and the non-Gaussian deviation shape is completely modified. The effect on the other two are milder, with the non-Gaussian deviation shapes more or less unaltered and a decrease in the amplitude of the deviations. This can be attributed to the fact that masking the new point sources leads to a decrease in the level of residual contamination. Earlier studies of the effects of contamination on the CMB have mostly focused on point sources [14, 15, 16, 17]. An investigation of the effect of point sources on MFs was done in [18].

This paper is organized as follows. In section 2 we present calculations of the correlations between the foreground and cleaned CMB maps and their statistical significance after applying point sources masks PS1, PS2 and PS3. In section 3, we compute MFs from Gaussian simulations to which a fraction of the foreground field is added and compare the non-Gaussian deviations to the corresponding deviations measured from WMAP 7 years data using PS1. We further study the effect of masking the additional point sources in PS2 and PS3 on the MFs. We end with concluding remarks in section 4.

2. Quantifying residual foreground contamination

We begin with the expectation that any two random fluctuation fields that originate from completely different physical processes will not have any correlation. Let f and f' be two random fields that have zero mean values, defined on the surface of a two dimensional sphere. Let their rms values be denoted by σ_0 and σ'_0 , respectively. By rescaling them as $\nu(i) \equiv f(i)/\sigma_0$ and $\nu'(i) \equiv f'(i)/\sigma'_0$, where i denotes the pixel number, we can define a correlation parameter, r , as

$$r \equiv \langle \nu(i) \nu'(i) \rangle, \quad (1)$$

where the bracket denotes average over all pixels. We expect r to be zero if the two fields are uncorrelated and non-zero otherwise. In numerical calculations we will always

get a non-zero value of r even for two fields that are known to be uncorrelated, due to the finite number of pixels, and we need to further test statistically whether the value is small enough to be considered as practically zero.

The observed WMAP data, f^{obs} , is a sum of the true CMB signal and foreground contamination. Let us call the foreground component that is estimated using a combination of galaxy observation and theoretical modeling, as the ‘apparent’ foreground field, denoted by f^{appfg} , keeping in mind that there may be small error in its estimation. This field is then subtracted pixel by pixel from f^{obs} to leave behind the ‘cleaned’ CMB signal, which we denote by f^{cleaned} . By definition, f^{cleaned} has zero mean. If f^{appfg} has been correctly estimated, then we expect it to have negligibly small correlation with f^{cleaned} , since they come from totally different physical processes. However, if the estimation is on the right track but not fully correct, then we should expect some residual contamination in the signal field. This should show up as non-zero correlation between f^{cleaned} and f^{appfg} .

2.1. Peak field

Our analysis is done using the 7 years data from the eight differential assemblies (DAs) of WMAP, namely, Q₁, Q₂, V₁, V₂, W₁, W₂, W₃ and W₄. For each DA the Galactic foreground is obtained from

$$f^{\text{appfg}} = f^{\text{obs}} - f^{\text{cleaned}}, \quad (2)$$

where ‘appfg’ indicates that f^{appfg} is the ‘apparent’ foreground and a fraction of it may be left behind in f^{cleaned} . To examine the existence of the residual foreground in the cleaned map we will compare the cleaned map with the foreground maps where the large-scale variation of the Galactic emissions is removed. A foreground map with the large-scale variation subtracted is called the *peak field* and is defined as

$$f^{\text{peak}} \equiv (f^{\text{appfg},\theta_s} - f^{\text{appfg},3\theta_s}) - \langle f^{\text{appfg},\theta_s} - f^{\text{appfg},3\theta_s} \rangle, \quad (3)$$

where θ_s and $3\theta_s$ are FWHM values at which we have smoothed the field. By definition f^{peak} has zero mean. The left panel of Fig. (1) shows the peak field for Q1 channel. In the right panel we have shown pixels (in white) of the same peak field which have values above $3\sigma^{\text{peak}}$.

To reduce the boundary effects by controlling the degree of masking we use the foreground mask map smoothed over FWHM= $3\theta_s$. The pixels of this map have value one well inside the mask boundaries and zero well outside, but have values between zero and one near the boundaries. The distance from the original mask boundaries is then encoded in the pixel values of the smoothed mask map. By using some threshold value, s_{mask} , of the smoothed mask pixels, we can control how far away we stay away from the mask boundary. Staying 2σ away from the boundary corresponds to choosing pixels with $s_{\text{mask}} > 0.89$. As we choose larger values of s_{mask} we stay further away from the boundaries and the sky fraction decreases.

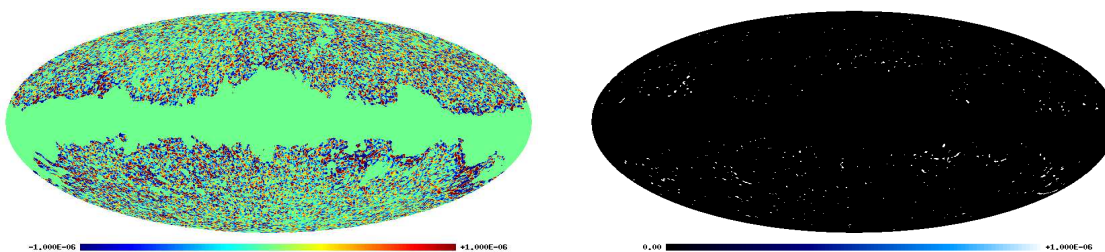


Figure 1. *Left panel:* Peak field for Q_1 DA. *Right panel:* Locations of pixels where the same peak field has values above $3\sigma^{\text{peak}}$ are shown in white.

	Q_1	Q_2	V_1	V_2	W_1	W_2	W_3	W_4
r_c for $s_{\text{mask}} = 0.89$	0.026	0.025	0.020	0.019	0.010	0.008	0.009	0.006
	0.018	0.018	0.017	0.016	0.009	0.008	0.007	0.007
r_c for $s_{\text{mask}} = 0.91$	0.025	0.025	0.020	0.019	0.009	0.007	0.008	0.006
	0.018	0.017	0.016	0.016	0.008	0.008	0.006	0.006
r_c for $s_{\text{mask}} = 0.93$	0.025	0.024	0.019	0.018	0.008	0.007	0.007	0.004
	0.017	0.017	0.016	0.015	0.007	0.007	0.005	0.006

Table 1. r_c values for the eight DAs are shown. Point sources mask used is PS1. For each DA and s_{mask} , the upper value gives r_c calculated using all unmasked pixels, while the lower value has been calculated after excluding pixels having $\nu^{\text{peak}} > 3$ also. The sky fractions for the three s_{mask} values from top to bottom are roughly 62%, 60% and 58%.

2.2. Correlation between peak and cleaned CMB fields

Let us denote

$$\nu^{\text{cleaned}}(i) \equiv \frac{f^{\text{cleaned}}(i)}{\sigma^{\text{cleaned}}}, \quad \nu^{\text{peak}}(i) \equiv \frac{f^{\text{peak}}(i)}{\sigma^{\text{peak}}}, \quad (4)$$

and define

$$r_c \equiv \langle \nu^{\text{cleaned}} \nu^{\text{peak}} \rangle_{\theta_s}, \quad (5)$$

where the suffix θ_s is to remind us that we do the calculation for a choice of FWHM at which f^{cleaned} has also been smoothed. σ^{cleaned} and σ^{peak} are of the orders of 10^{-5} and 10^{-7} , respectively. Table (1) summarizes the main results for r_c where point sources mask PS1 has been used. We have chosen $\theta_s = 35'$ based on the resolution of Q_1 channel. Two values of r_c are shown for each DA and s_{mask} . The upper value is the case where r_c is calculated using all unmasked pixels, while the lower value is the case where pixels with $\nu^{\text{peak}} > 3$, shown in the right panel of Fig. (1) for Q_1 , have been excluded. The first observation we make is that *all* r_c values are positive. For Q channels *we get*

	Q_1	Q_2	V_1	V_2	W_1	W_2	W_3	W_4
N for	0	0	5	8	120	169	139	224
$s_{\text{mask}} = 0.89$	14	14	105	114	276	276	314	303
N for	0	0	7	10	136	193	160	255
$s_{\text{mask}} = 0.91$	15	16	110	122	284	286	338	318
N for	0	0	14	14	161	219	199	294
$s_{\text{mask}} = 0.93$	18	20	121	130	295	294	350	342

N_0 for	0
$s_{\text{mask}} = 0.89$	13
N_0 for	0
$s_{\text{mask}} = 0.91$	15
N_0 for	0
$s_{\text{mask}} = 0.93$	18

Table 2. *Left:* Number of maps, N , having $r_g > r_c$ for individual DAs, out of 1000 Gaussian maps for PS1. As in Table (1), upper values are for all unmasked pixels included, while lower values are for the case when pixels with $\nu^{\text{peak}} > 3$ have also been excluded. *Right:* Number of Gaussian maps, N_0 , having $r_g > r_c$ simultaneously for all DAs.

considerably larger correlation when we keep all unmasked pixels, larger by about 30%. This indicates that there is non-trivial correlation arising from the pixels with $\nu^{\text{peak}} > 3$. For V channels the difference is about 20% while W channels don't seem to be affected. The sky fractions for the three s_{mask} values are roughly, 62%, 60% and 58%, respectively. For Q and V channels, as we stay further away from the mask boundaries there is small but systematic decrease of r_c .

2.3. Statistical significance of r_c values

We investigate how likely it is to get the observed r_c values given in Table (1) by comparing with correlations between the peak field and Gaussian CMB simulations. For this purpose we simulate 1000 Gaussian CMB maps with WMAP 7 years parameter values, add pixel window effect, beam smearing and WMAP 7 years noise characteristics. Next we smooth by FWHM 35' and mask in exactly the same way as we did when calculating r_c and calculate the correlation with the peak field. We denote the correlation value by r_g . The Gaussian fields are uncorrelated with the signal field and we should get small value of r_g . This exercise will tell us what is the typical value of 'small' r_c that we can approximate to be zero for the number of pixels under consideration and how likely are our observed r_c values to occur by random fluctuation and not due to a true correlation.

We count, out of the thousand r_g values, how many are greater than r_c . The results are shown in Table (2). The left table shows the number, N , of Gaussian maps having $r_g > r_c$ for each individual DA, for the three s_{mask} values used earlier for calculating r_c and including/excluding the pixels having $\nu^{\text{peak}} > 3$. When all unmasked pixels are included, we get $N = 0$ for all s_{mask} values for Q channel, for V channels N lies between 5 and 14, while for W channels N lies between 120 and 294. These numbers imply that the r_c values for Q and V are statistically significant, whereas, the values for W

	Q_1	Q_2	V_1	V_2	W_1	W_2	W_3	W_4
r_c for $s_{\text{mask}} = 0.89$	0.013	0.013	0.010	0.010	0.002	0.001	0.001	-0.001
	0.010	0.009	0.009	0.009	0.005	0.005	0.003	0.003
r_c for $s_{\text{mask}} = 0.91$	0.013	0.013	0.010	0.009	0.002	0.001	0.001	-0.002
	0.010	0.009	0.009	0.009	0.005	0.004	0.002	0.002
r_c for $s_{\text{mask}} = 0.93$	0.012	0.012	0.009	0.009	0.001	-1×10^{-6}	-4×10^{-5}	-0.003
	0.009	0.009	0.009	0.008	0.004	0.003	0.001	0.002

Table 3. r_c values for the eight DAs after applying PS2. Y As in Table (1), for each DA and s_{mask} , the upper value gives r_c calculated using all unmasked pixels, while the lower value has been calculated after excluding pixels having $\nu^{\text{peak}} > 3$ also. The sky fractions for the three s_{mask} values from top to bottom are roughly 61%, 59% and 57%.

	Q_1	Q_2	V_1	V_2	W_1	W_2	W_3	W_4
N for $s_{\text{mask}} = 0.89$	37	39	148	159	407	462	448	549
	157	163	269	280	384	396	442	430
N for $s_{\text{mask}} = 0.91$	39	43	158	167	430	482	475	584
	164	167	285	292	392	407	458	448
N for $s_{\text{mask}} = 0.93$	45	46	166	168	449	505	511	628
	173	175	293	301	406	416	477	470

N_0 for $s_{\text{mask}} = 0.89$	35
	148
N_0 for $s_{\text{mask}} = 0.91$	38
	154
N_0 for $s_{\text{mask}} = 0.93$	43
	162

Table 4. *Left:* Number of maps, N , having $r_g > r_c$ for individual DAs, out of 1000 Gaussian maps, calculated after applying PS2. As in Table (2), upper values are for all unmasked pixels included, while lower values are for the case when pixels with $\nu^{\text{peak}} > 3$ have also been excluded. *Right:* Number of Gaussian maps, N_0 , having $r_g > r_c$ simultaneously for all DAs.

channels have much lower significance. When pixels with $\nu^{\text{peak}} > 3$ are also excluded, we find a reduction of N for all the channels. The table on the right side of Table (2) shows the number, N_0 , of Gaussian maps having $r_g > r_c$ *simultaneously for all DAs*. These values are again significant. Therefore, we conclude that the cleaned WMAP data, particularly Q and V channels, contain small but statistically significant amount of residual foreground contamination.

2.4. Correlation between peak and cleaned CMB fields after applying extended point sources masks PS2 and PS3

We have repeated the calculation of r_c and the analysis of the statistical significance after masking after applying PS2. Masking the new point sources results in a further decrease of roughly 1% of the sky fraction. The r_c values that we obtain are shown in Table (3). The significance test results are shown in Table (4). We find a clear decrease in the correlation values and their statistical significance which indicates that there is reduction in the residual contamination, as should be expected .

3. Minkowski Functionals and residual foreground

The morphological properties of excursions sets of the CMB (the set of all pixels having temperature fluctuation values greater than or equal to some threshold value, ν) can be neatly captured by the so called Minkowski Functionals. There are three MFs that are relevant for the CMB. The first is the area fraction, V_0 , of the excursion set, the second is the total length, V_1 , of iso-temperature contours or boundaries of the excursion sets and the third is the genus, V_2 , which is the difference between the numbers of hot and cold spots [12]. For a Gaussian random field the MFs are given by,

$$V_k(\nu) = A_k H_{k-1}(\nu) e^{-\nu^2/2}, \quad k = 0, 1, 2. \quad (6)$$

$H_n(\nu)$ is the n -th Hermite polynomial and the amplitude A_k depends only on the angular power spectrum C_l . It is given by

$$A_k = \frac{1}{(2\pi)^{(k+1)/2}} \frac{\omega_2}{\omega_{2-k}\omega_k} \left(\frac{\sigma_1}{\sqrt{2}\sigma_0} \right)^k, \quad (7)$$

$$\sigma_j^2 \equiv \frac{1}{4\pi} \sum_l (2l+1) [l(l+1)]^j C_l W_l^2, \quad (8)$$

with $\omega_k \equiv \pi^{k/2}/\Gamma(k/2+1)$. σ_1 is the rms of the gradient of the field and W_l represents the smoothing kernel determined by the pixel and beam window functions and any additional smoothing. The presence of any small deviation from Gaussianity will appear as deviations from these formulas. The MFs are useful because they have characteristic non-Gaussian deviation shapes for different types of non-Gaussianity and can distinguish them. They carry information of all orders of n -point functions and this makes them unbiased towards specific forms of non-gaussianity.

For the numerical computation of MFs for any given random field we use the method described in [19]. This method was shown to have numerical inaccuracies which are of specific forms arising from the finite approximation of the delta function and which scales as the square of the finite binning of the temperature threshold values at leading order [20]. In our calculations we estimate and subtract these inaccuracies and we denote the corrected result by V_i^{NG} . For weakly non-Gaussian fields we can obtain the Gaussian component by using the formula Eq. (6) where the amplitude is computed by

measuring σ_0 and σ_1 directly from the field. We denote it by V_i^G . The non-Gaussian deviation is then given by

$$\Delta V_i \equiv V_i^{NG} - V_i^G. \quad (9)$$

3.1. Effect of residual contamination on Minkowski Functionals

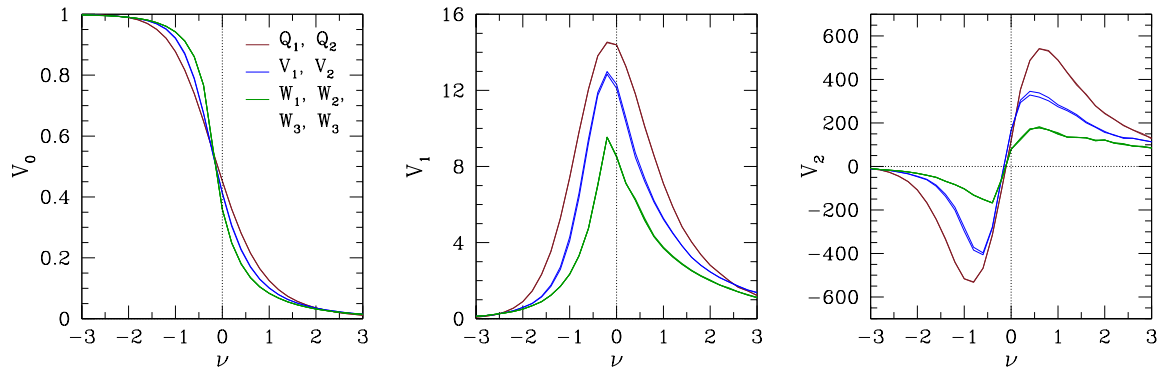


Figure 2. Minkowski functionals for the peak fields.

In this subsection we study how the residual foreground contamination affects the MFs. We begin by examining the shapes of the MFs for the peak fields shown in Fig. (2) for each of the DAs. It is obvious that they have strong departures from Gaussian shapes. We can therefore expect that if any small fraction of the peak fields contaminate the CMB field it will show up as non-Gaussian deviation in the MFs.

In order to mimic and quantify the effect of the residual contamination on the MFs we add ϵf^{peak} to Gaussian simulated maps, as,

$$f^{\text{contaminated}} = f^G + \epsilon f^{\text{peak}}, \quad (10)$$

where f^G is the simulated Gaussian map, to which we have added instrumental effects, as described in section (2.3). Note that the largest contribution to the non-Gaussian deviation of the MFs arising from non-zero ϵ will scale linearly with it [21]. The MFs and their non-Gaussian deviations (yellow dots) computed from $f^{\text{contaminated}}$, averaged over 1000 maps, are shown in Fig. (3). We have chosen values of ϵ which result in amplitudes of the MFs similar to the observed ones. The ϵ value used for these plots is $\epsilon = 8r_c/(r_c + \sigma^{\text{peak}}/\sigma^{\text{cleaned}})$ for each respective DA. In the same figure we have also shown the ΔV_i computed from the WMAP 7 years data (red dots) after applying PS1. As seen in the figure, there is remarkable agreement between the two plots. We infer that most of the non-Gaussian deviation that we measure in the WMAP data is contributed by residual foreground contamination.

3.2. Effect of PS2 and PS3 on Minkowski Functionals from WMAP

We calculate the MFs for WMAP 7 years data after applying PS2 and PS3. The non-Gaussian deviations are shown in Fig.(4), along with the result of PS1 so as to compare

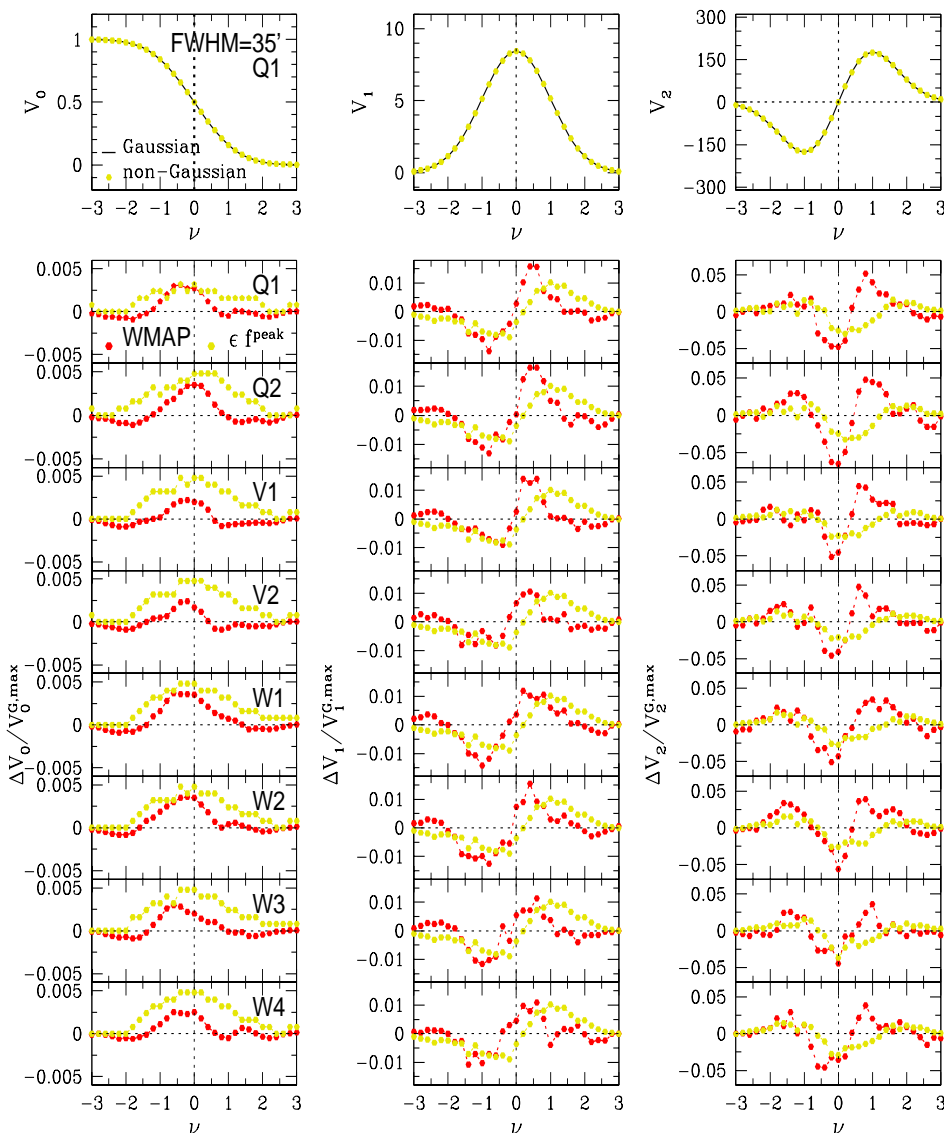


Figure 3. Minkowski Functionals and their non-Gaussian deviations (Eq. (9)), measured from Gaussian simulations to which residual contaminant fraction has been added, given by Eq. (10). Average over 1000 simulations.

the three. The Galaxy mask applied is KQ75 as done in previous sections. We find that $\Delta V_0(\nu)$ is strongly affected by the removal of the new point sources, it flips sign. This is simple to understand, as explained below. Let N denote the total number of unmasked pixels. At any ν let us denote the number of pixels greater than or equal to ν by $n(\nu)$. $V_0(\nu)$ is given by $n(\nu)/N$. When we mask new point sources we exclude, say m , positive valued pixels. Then the effect of the new masking gives new value $V'_0(\nu)$. Since m is positive, this implies $V'_0(\nu) < V_0(\nu)$. If we started with V_0 which is greater than the Gaussian value and this decrease makes V'_0 less than the Gaussian value, then ΔV_0 will flip sign which is the case here. This suggests that $V_0(\nu)$ is unreliable for extraction

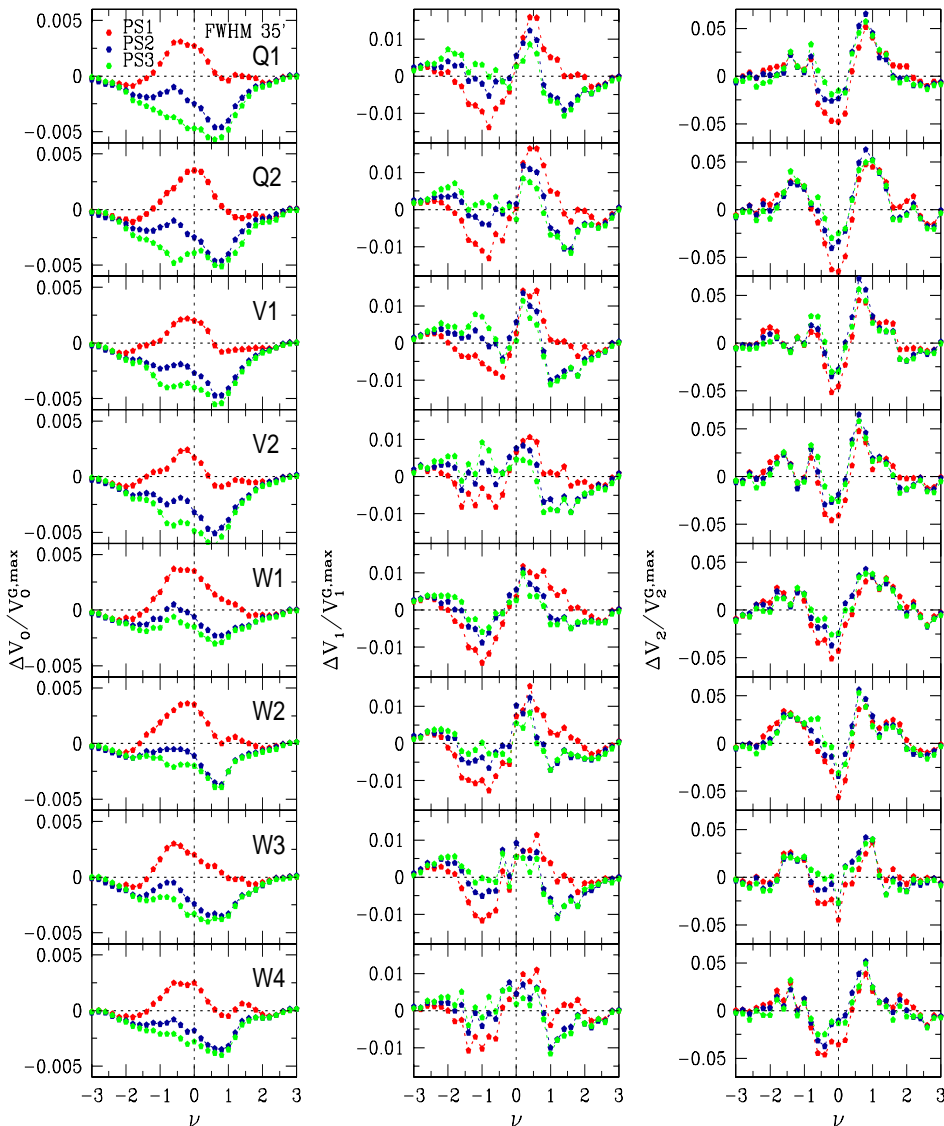


Figure 4. Non-Gaussian deviations of Minkowski functionals for the eight DAs of WMAP 7 years data for the three cases where point sources masks PS1, PS2 and PS3 were applied.

of non-Gaussianity information due to our imprecise knowledge of point sources in the sky. For $\Delta V_1(\nu)$ the amplitude is decreased considerably but the shape is more or less unaffected. The genus is affected the least and the main effect is a reduction of the non-Gaussian deviation around $\nu = 0$. These effects are due to the reduction in the level of contamination due to the masking of the new point sources.

4. Conclusion

We have analysed the cleaned WMAP 7 years data with the goal of quantifying the amount of residual foreground contamination outside the Galactic and point sources

masks and the resulting bias in the estimates of primordial non-Gaussianity by using Minkowski Functionals. The presence of significant residual contamination is confirmed by calculations of correlations between the cleaned maps and the foreground maps which give values that are found to be statistically significant. The Q channel is found to have the strongest correlations and hence largest residual contamination while W channel has the least. For Q and V channels we found that a big fraction of the contamination come from pixels where the foreground fields have large values. A comparison of the correlation and significance values obtained after applying the point sources mask provided by WMAP and the extended masks of Scodeller *et al.* reveals that the extended masks remove some fraction of the residual contamination, as should be expected.

The above results have important implications for the extraction of cosmological parameters from observational data, particularly on the search for primordial non-Gaussianity, using the cleaned WMAP data. In order to understand the implications we simulate contaminated CMB maps by adding a fraction of the foreground field to Gaussian maps and measure Minkowski Functionals from them. The non-Gaussian deviation shapes of all the three MFs are found to have remarkable agreement with what is measured from the cleaned WMAP data after applying PS1. Non-Gaussian deviations of MFs calculated after applying PS2 and PS3 give a reduction in the overall magnitude of the deviations compared to PS1. ΔV_0 actually changes sign owing to its strong sensitivity to point sources and is not reliable to be used for constraining primordial non-Gaussianity. The shapes of ΔV_1 and ΔV_2 are relatively insensitive to the different masking with the main effect being a decrease in the amplitude. These results are consistent with a reduction in the level of residual contamination.

We conclude that the cleaned WMAP 7 years data contains significant amount of residual foreground contamination, both from diffuse Galactic emissions and unresolved extra-Galactic point sources. Note that more than 15000 point sources have already been identified from data from the PLANCK satellite [23]. A rough visual comparison between the amplitudes of ΔV_i in Figs. (3) and (4) and the corresponding amplitudes of deviations due to the local primordial non-Gaussianity parameter f_{NL} [21] tells us that the cleaned data contains residual contamination of similar levels as $f_{\text{NL}} > 100$. Unless this is removed the constraints put on primordial non-Gaussianity parameters, such as in [22], are not sensible. Our calculations may be refined to obtain a good estimate of the residual contamination fraction encoded in the parameter ϵ . It can then be further subtracted from the cleaned data and the resulting maps can be used to search for primordial non-Gaussianity. It is also imperative that we redo such analysis after applying the extended point sources masks PS2 and PS3. We are currently initiating this investigation.

Acknowledgment

We thank Korea Institute for Advanced Study for providing computing resources (KIAS Center for Advanced Computation Linux Cluster System QUEST) where a part of the

computation was carried out. We acknowledge use of the HEALPIX package. We acknowledge the use of the Legacy Archive for Microwave Background Data Analysis (LAMBDA). Support for LAMBDA is provided by the NASA Office of Space Science.

References

- [1] E. Komatsu, *et. al.*, ApJS, 192, 18 (2011)
- [2] J. Kim, C. Park, G. Rossi, S. M. Lee and J. R. Gott, JKAS, 44, 217 (2011)
- [3] J.-C. Hwang, JKAS, 45, 65 (2012)
- [4] L. Toffolatti, F. Argeso Gomez, G. De Zotti, P. Mazzei, A. Franceschini, L. Danese and C. Burigana, Mon. Not. Roy. Astron. Soc. **297**, 117 (1998) [astro-ph/9711085].
- [5] B. Gold, *et.al.*, ApJS, 192, 15 (2011).
- [6] <http://lambda.gsfc.nasa.gov/>
- [7] S. Scodeller, F. K. Hansen and D. Marinucci, Astrophys. J. **753**, 27 (2012) [arXiv:1201.5852 [astro-ph.CO]].
- [8] S. Scodeller and F. K. Hansen, arXiv:1207.2315 [astro-ph.CO].
- [9] P. Chingangbam and C. Park, submitted to Journal of Physics Conference Series.
- [10] H. Tomita, Progr. Theor. Phys. **76**, 952 (1986).
- [11] P. Coles, Mon. Not. Roy. Astron. Soc. **234**, 509 (1988).
- [12] J. R. Gott, C. Park, R. Juzkiewicz, W. E. Bies, F. R. Bouchet and A. Stebbins, Astrophys. J. **352**, 1 (1990).
- [13] S. Winitzki and A. Kosowsky, New Astron. **3**, 75 (1998) [arXiv:astro-ph/9710164].
- [14] F. Argueso, J. Gonzalez-Nuevo and L. Toffolatti, 2003 ApJ **598** 86
- [15] S. P. Boughn, R. B. Partridge, 2008, PASP **120**, No. 865 2008, Publications of the Astronomical Society of the Pacific **120**, No. 865
- [16] D. Babich and E. Pierpaoli, 2008, Phys. Rev. D **77**, 123011 (2008)
- [17] F. Lacasa, N. Aghanim, M. Kunz and M. Frommert, arXiv:1107.2251 [astro-ph.CO].
- [18] D. Munshi, P. Coles and A. Heavens, arXiv:1207.6217 [astro-ph.CO].
- [19] J. Schmalzing and K. M. Gorski, astro-ph/9710185.
- [20] E. A. Lim and D. Simon, J. Cosmol. Astropart. Phys., 1, 48 (2012)
- [21] C. Hikage, E. Komatsu and T. Matsubara, Astrophys. J. **653**, 11 (2006) [arXiv:astro-ph/0607284].
- [22] C. Hikage and T. Matsubara, arXiv:1207.1183 [astro-ph.CO].
- [23] Planck Collaboration, Planck early results. VII. The Early Release Compact Source Catalogue, A&A 536, A7 (2011)